Homogeneous nucleation rate measurements in supersaturated water vapor

David Brus,[1,2,a)] Vladimír Ždímal,[1] and Jiří Smolík[1]

[1]*Laboratory of Aerosol Chemistry and Physics, Institute of Chemical Process Fundamentals AS CR, v.v.i., Rozvojová 135, CZ-16502 Prague, Czech Republic*
[2]*Finnish Meteorological Institute, Erik Palménin aukio 1, P.O. Box 503, FI-00101 Helsinki, Finland*

The rate of homogeneous nucleation in supersaturated vapors of water was studied experimentally using a thermal diffusion cloud chamber. Helium was used as a carrier gas. Our study covers a range of nucleation rates from 3×10^{-1} to 3×10^{2} cm^{-3} s^{-1} at four isotherms: 290, 300, 310, and 320 K. The molecular content of critical clusters was estimated from the slopes of experimental data. The measured isothermal dependencies of nucleation rate of water on saturation ratio were compared with the prediction of the classical theory of homogeneous nucleation, the empirical prediction of Wölk *et al.* [J. Chem. Phys. **117**, 10 (2002)], the scaled model of Hale [Phys. Rev. A **33**, 4156 (1986)], and the former nucleation onset data. © *2008 American Institute of Physics.*
[DOI: 10.1063/1.3000629]

INTRODUCTION

Nucleation is a critical step in vapor to liquid phase transition. In most situations the heterogeneous nucleation is important, that occurs under the presence of foreign nuclei, aerosol particles, ions, or surfaces. If they are absent, the process takes place by vapor condensation on its own embryos. This process is termed homogeneous nucleation and in unary vapor it represents the simplest system for both experimental and theoretical investigations of nucleation. The water vapor plays a significant role in the Earth's atmosphere. It participates in nucleation of more complex binary and ternary systems as water-sulfuric acid plus surface-active organic substances such as ammonia or dimethylamine that lower the surface tension and enhance the nucleation process.[1] Water vapor is the most potent greenhouse gas influencing strongly both the incoming and the outgoing radiation. Water vapor moderates the Earth's climate by buffering large fluctuations in temperature.

Most of the available data on the homogeneous nucleation of water were produced by devices using adiabatic expansion (Wilson, Volmer and Flood, Allen and Kassner, Wagner and Strey, Miller *et al.*; Peters, Viisanen, Viisanen *et al.*, Luijten *et al.*, Schmitt *et al.*, Viisanen *et al.*, Wölk *et al.*, Wölk and Strey 2001, Heath *et al.*, and Holten *et al.*);[2–16] only several studies used devices based on nonisothermal diffusion of studied vapor through an inert gas (Heist and Reiss, Mirabel and Katz, Chukanov and Kuligin, Beloded *et al.*, and Mikheev *et al.* 2002).[17–21]

Generally, the diffusion based devices, often called the diffusion chambers, are used both for the determination of critical supersaturation and for nucleation rate measurements. In these studies, the nucleation rate is usually derived from the integral flux of droplets recorded by an optical counter. The inherent presence of nonuniformities in temperature and supersaturation, and the way of droplets detection cause difficulties in comparing the results from diffusion chambers with the results obtained by other techniques. Several years ago, the method of droplets detection in the thermal diffusion cloud chamber (TDCC) was modified.[22] This approach allowed us to determine the rate of nucleation, and its dependence on temperature and supersaturation, independently on any nucleation theory. Here this technique is used to measure the homogeneous nucleation rate in supersaturated vapors of water in helium at four temperatures: 290, 300, 310, and 320 K.

In 1973, Heist and Reiss[17] reported the first onset nucleation data, sometimes called critical supersaturations, in a thermal diffusion chamber. 35 years later we bring to the nucleation community a first set of the experimental nucleation rate data from the same device. The obtained data are compared both with the theoretical predictions and with all available data of others.

EXPERIMENTAL METHOD

The TDCC used in this work was first presented in detail elsewhere.[23] A short overview of the technique is given here. The basic function of the TDCC is to produce supersaturated vapor by using nonisothermal diffusion. The chamber is designed so that one-dimensional diffusion of vapor takes place through an inert carrier gas. The chamber consists of two circular duraluminum plates, separated by a 25 mm high ring made of 5 mm thick optical glass with an inner diameter of 160 mm. The effective diameter to height (the distance between liquid films) ratio is 7:1. To minimize the wall effect, the ring is wrapped by six equally spaced resistance wires, in parallel connection, connected to one power supply. The required unequal heating of the wall is reached by suitable choice of wires of different resistivities. The bottom plate covered with a thin film (less than 1 mm) of studied liquid is

a)Electronic mail: brus@icpf.cas.cz.
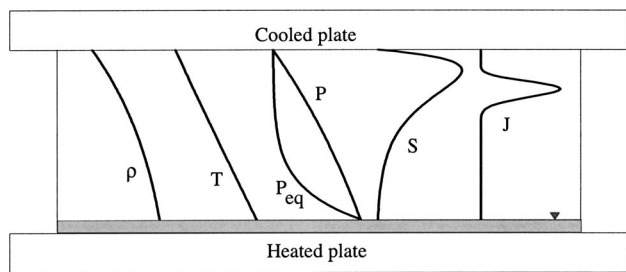
FIG. 1. The schematic picture of the calculated profiles inside the TDCC.

heated. Vapor of the studied substance evaporates from the film surface, diffuses through an inert gas, and condenses on the cooler top plate. The condensate flows along the glass wall back to the pool, so that the chamber can be operated at a steady state. The type and pressure of the inert gas are chosen so that the density profile is stable against buoyancy driven convection. Under such circumstances, the character of transport processes between the plates leads to a state, where both the temperature T and the partial vapor pressure p decrease almost linearly with the increasing chamber height, see Fig. 1. Since the equilibrium vapor pressure p_{eq} decreases with the height more quickly than p, the vapor in the chamber becomes supersaturated with a maximum supersaturation $S=p/p_{eq}$ reached close to the top plate. By increasing the temperature difference between both plates, the supersaturation can be increased until it is sufficient for homogeneous nucleation to start. Temperatures of the liquid surfaces are not measured directly but temperatures of the plates are measured instead, the temperatures of the liquid surfaces have to be calculated. It is assumed that the heat conduction is the main mechanism of heat transport through the films.[23] The self-cleaning nature of the chamber hinders heterogeneous nucleation. The nucleation induced by ions is effectively prevented by applying an electrostatic field (80 V cm^{-1}) across the chamber. Stable clusters of the new

phase are formed and then grow rapidly to become visible droplets; all this happens inside a thin layer called a nucleation zone (spanning over about 10% of chamber height) with nucleation rate maximum located somewhat below the supersaturation maximum. The formed droplets fall back to the liquid film due to gravity.

The method of precise determination of the nucleation rate is described in detail in the paper of Brus *et al.*[24] It uses a charge coupled device (CCD) camera to record droplet trajectories online and the algorithms of image analysis to determine vertical positions of nucleated droplets on digital images. After evaluating a sufficient number of visible droplets (starting points) in one experiment, we obtain their number distribution as a function of the chamber height. By dividing the number distribution by the photographed volume and the exposure time we get the homogeneous nucleation rate (as droplets per cubic centimeter per second) as a function of the height in the chamber. The homogenous nucleation rate distribution is subsequently fitted by a Gaussian distribution. This method presents the experimentally determined homogeneous nucleation rate $J_{exp}(z)dz$ as a function of vertical position inside the chamber, z. These local values of nucleation rate are then related to the corresponding values of temperature and supersaturation, as calculated using a one-dimensional model of mass and heat transport in the TDCC,[25,26] see Fig. 2. The resulting dependence $J_{exp}(T,S)$ is directly comparable to the theoretical prediction of any nucleation theory.

In this study we used a purified water (ULTRAPURE, Watrex s.r.o, electrical conductivity $< 0,1$ μS/cm, TOC < 10 parts per billion) as the condensing vapor and helium (Linde, purity of 99.996%) as the carrier gas. The physico-chemical properties of water and helium are presented in Table I. The error analysis, short overview, and comments to
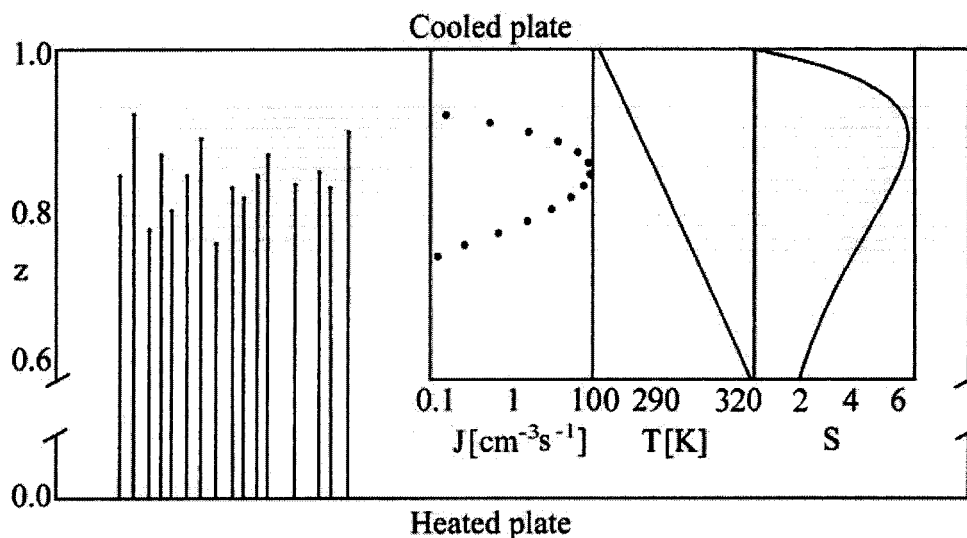
FIG. 2. The illustration of the experimental data evaluation method in the TDCC. Typical trajectories of droplets recorded by the CCD camera are shown on the left side of the figure in relation to the dimensionless height z of the chamber. In the three windows of the insert we see the experimentally determined local homogeneous nucleation rate J, and calculated vertical profiles of temperature T, and supersaturation S, all as functions of dimensionless height of the chamber, z.

TABLE I. Physicochemical properties of helium, water, and the mixture of water-helium. M is the molar mass, σ and ε/k the force constants for the Lennard-Jones (6–12) potential in m and K, respectively, c_p the heat capacity, λ the thermal conductivity, η the viscosity, $\Omega^{(i,j)}$ the collision integral of the type (i,j) as defined in Hirschfelder *et al.*, T the temperature in K, T_c the critical temperature, T_b the temperature of the normal boiling point, P_{eq} the equilibrium vapor pressure, P the total pressure, P_c the critical pressure, γ the surface tension, ΔH the enthalpy of vaporization, D_{ab} the binary diffusion coefficient, α the thermal diffusion factor, x the molar fraction, A the factors in the Wassiljewa equation estimated by Mason–Saxena method (Reid *et al.*), and k the Boltzmann constant. Indexes: v—vapor, g—gas, vg—vapor-gas mixture, l—liquid.

Property	Equation	Unit	Ref.
	Helium		
M_g	4.0026	kg kmol^{-1}	37
σ_g	2.551×10^{-10}	m	37
ε_g/k	10.22	K	37
c_p	20.786	J mol^{-1} K^{-1}	37
λ_g	$(-5.8543\times10^{-5}+2.686\,06\times10^{-6}\times T-7.001\,13\times10^{-9}\times T^2+1.073\,96\times10^{-11}\times T^3-6.017\,68\times10^{-15}\times T^4)\times4.1868\times100$	W m^{-1} K^{-1}	38
η_g	$1.4083\times10^{-6}T^{1.5}/(T+70.22)$	Pa s	44
	Water		
M_v	18.015	kg kmol^{-1}	37
σ_v	2.641×10^{-10}	m	37
ε_v/k	809.1	K	37
T_b	373.15	K	37
T_c	647.14	K	37
P_c	$22.064\times10^{+6}$	Pa	37
$C_{p,v}$	$4186.8(7.701+4.595\times10^{-4}T+2.521\times10^{-6}T^2-0.859\times10^{-9}T^3)$	J kmol^{-1} K^{-1}	37
λ_v	$418.68(-1.6487\times10^{-5}+1.9895\times10^{-7}T)$	W m^{-1} K^{-1}	44
λ_l	0.600	W m^{-1} K^{-1}	37
ρ_l	$1000(1.0-((T-273.15)-3.9863)^2((T-273.15))+288.9414)/(508\,929.2((T-273.15)+68.129\,63)))$	kg m^{-3}	43
γ_l	$93.663\times10^{-3}+9.133\times10^{-6}T-2.75\times10^{-7}T^2$	N m^{-1}	42
P_v^{eq}	$133.322(10^a)$, where $a=19.301\,142-2892.3693/T-2.892\,736$ log $10(T)-4.936\,972\,8\times10^{-3}T+5.606\,905\times10^{-6}T^2-4.645\,869\times10^{-9}T^3+3.7874\times10^{-12}T^4$	Pa	42
ΔH_v	40.68×10^6	J kmol^{-1}	40
	Mixed Properties		
D_{vg}	$2.663\times10^{-22}T^{1.5}((M_v+M_g)/(2M_vM_g))^{0.5}/(P\sigma_{vg}^2\Omega_{vg}^{(i,j)}\times(kT/\varepsilon_{vg}))$	m^2 s^{-1}	41
$1/\alpha$	$[-1.042\,67-T/(33.7629-0.358\,55\times T)]\times(xv+0.610\,43)+0.636\,48$	1	39
λ_{vg}	$x_v\lambda_v/(x_v+A_{vg}x_g)+x_g\lambda_g/(x_g+A_{gv}x_v)$	W m^{-1} K^{-1}	37
σ_{vg}	2.596×10^{-10}	m	37
ε_{vg}/k	90.93	K	37

the key water physicochemical properties used in homogeneous nucleation studies until the present time are provided in supplementary material online.[27]

RESULTS AND DISCUSSION

Homogeneous nucleation rates of water in helium were measured ranging from 3×10^{-1} to 3×10^2 cm^{-3} s^{-1} in two sets of measurements to ensure reproducibility of results. The lower limit of the TDCC is caused by the difficulties in running very long experiments (many hours) and the higher limit due to vapor depletion and latent heat release. The nucleation temperatures studied in this paper covered the range from 290 to 320 K in steps of 10 K. The lower temperature limit is given by the freezing point temperature at the cooled top plate of the chamber. The highest operating temperature is limited by the boiling point temperature of the chamber's bottom plate, corresponding to the operating pressure. In order to avoid buoyancy driven convection inside the TDCC, the total pressure must remain below some limiting value that depends on the temperature, condensable vapor, and background gas.[28,29] The pressure in the TDCC was varied from 50 kPa at $T_{nucl}=290$ K to 170 kPa at $T_{nucl}=320$ K. In this work, we did not test whether the helium pressure has an influence on the measured nucleation rate due to a very narrow total pressure range available.

The obtained experimental nucleation rate data are presented in Table II for both sets of measurements. The nucle-

TABLE II. The nucleation rates of water in helium. T_b is temperature of the bottom plate, T_t is temperature of the top plate, T_{nucl} is nucleation temperature, p_{tot} is total pressure, S_{nucl} is the supersaturation at T_{nucl}, and J_{exp} is the experimental nucleation rate.

T_b (K)	T_t (K)	T_{nucl} (K)	p_{tot} (kPa)	S_{nucl}	J_{exp} (cm^{-3} s^{-1})
		The first set of measurements			
$T = 290$ K					
332.04	273.08	290	51.73	3.91	$1.39 \times 10^{+01}$
332.21	273.12	290	51.98	3.93	$1.73 \times 10^{+01}$
333.17	274.18	290	52.26	3.94	$1.57 \times 10^{+01}$
333.30	274.18	290	52.28	3.96	$1.44 \times 10^{+01}$
333.44	274.16	290	52.46	3.98	$2.36 \times 10^{+01}$
333.57	274.13	290	52.64	4.00	$2.59 \times 10^{+01}$
333.90	274.07	290	53.07	4.05	$4.17 \times 10^{+01}$
334.20	274.01	290	53.32	4.10	$5.48 \times 10^{+01}$
333.81	274.06	290	51.15	4.06	$6.65 \times 10^{+01}$
334.19	274.08	290	51.51	4.12	$1.12 \times 10^{+02}$
334.52	274.06	290	51.74	4.17	$1.63 \times 10^{+02}$
334.72	274.04	290	51.98	4.20	$1.08 \times 10^{+02}$
331.77	273.89	290	50.48	3.79	$1.10 \times 10^{+00}$
332.31	273.74	290	53.22	3.85	$2.03 \times 10^{+00}$
332.15	273.81	290	53.15	3.82	9.54×10^{-01}
331.99	273.84	290	53.15	3.80	$1.27 \times 10^{+00}$
335.38	275.13	290	52.65	4.14	$7.86 \times 10^{+01}$
335.15	375.12	290	52.46	4.11	$5.46 \times 10^{+01}$
334.60	275.10	290	52.18	4.03	$2.27 \times 10^{+01}$
$T = 300$ K					
344.77	282.20	300	112.50	3.61	$3.32 \times 10^{+01}$
344.91	282.15	300	112.76	3.64	$4.42 \times 10^{+01}$
345.15	282.11	300	112.98	3.67	$6.48 \times 10^{+01}$
345.40	282.07	300	113.17	3.70	$8.61 \times 10^{+01}$
345.55	282.02	300	113.26	3.73	$1.10 \times 10^{+02}$
345.83	281.95	300	113.52	3.77	$1.34 \times 10^{+02}$
345.97	281.94	300	113.60	3.79	$1.80 \times 10^{+02}$
344.83	281.94	300	116.30	3.63	$1.80 \times 10^{+01}$
344.48	281.95	300	116.30	3.59	$1.00 \times 10^{+01}$
344.20	281.98	300	115.88	3.55	$7.73 \times 10^{+00}$
344.09	281.97	300	115.83	3.54	$7.33 \times 10^{+00}$
343.90	281.99	300	115.67	3.52	$1.79 \times 10^{+00}$
343.82	283.18	300	109.90	3.41	6.65×10^{-01}
343.67	283.22	300	109.65	3.39	$1.04 \times 10^{+00}$
343.58	283.20	300	109.74	3.39	7.98×10^{-01}
$T = 310$ K					
353.55	291.77	310	131.12	3.17	$1.95 \times 10^{+01}$
353.70	291.78	310	131.31	3.18	$1.31 \times 10^{+01}$
353.93	291.73	310	131.55	3.21	$2.03 \times 10^{+01}$
354.17	291.77	310	131.88	3.23	$2.37 \times 10^{+01}$
354.33	291.68	310	132.08	3.25	$3.60 \times 10^{+01}$
354.46	291.74	310	132.29	3.26	$4.76 \times 10^{+01}$
354.61	291.72	310	132.40	3.27	$6.36 \times 10^{+01}$
354.77	291.67	310	132.64	3.29	$7.85 \times 10^{+01}$
354.92	291.62	310	132.81	3.31	$1.18 \times 10^{+02}$
355.04	291.59	310	132.93	3.33	$1.34 \times 10^{+02}$
355.18	291.57	310	132.21	3.35	$1.45 \times 10^{+02}$
353.51	291.49	310	134.23	3.18	$9.55 \times 10^{+01}$
353.29	291.42	310	133.90	3.16	$1.72 \times 10^{+01}$
353.11	291.43	310	133.69	3.14	$6.30 \times 10^{+00}$
352.95	291.45	310	133.50	3.13	$4.96 \times 10^{+00}$
352.68	291.46	310	133.20	3.10	$3.24 \times 10^{+00}$
352.44	291.48	310	132.90	3.08	$2.10 \times 10^{+00}$
352.34	291.25	310	133.41	3.08	$1.30 \times 10^{+00}$

TABLE II.   (*Continued.*)

		The first set of measurements			
T_b (K)	T_t (K)	T_{nucl} (K)	p_{tot} (kPa)	S_{nucl}	J_{exp} (cm^{-3} s^{-1})
352.08	291.27	310	133.09	3.06	$3.30 \times 10^{+00}$
T=320 K					
364.85	300.89	320	171.95	3.01	$2.37 \times 10^{+02}$
364.62	300.93	320	171.61	2.99	$1.81 \times 10^{+02}$
364.42	300.95	320	171.21	2.97	$1.59 \times 10^{+02}$
364.11	300.97	320	170.72	2.94	$1.17 \times 10^{+02}$
363.80	301.02	320	170.18	2.92	$7.96 \times 10^{+01}$
363.61	301.18	320	169.70	2.89	$4.59 \times 10^{+01}$
363.29	301.24	320	169.16	2.86	$1.93 \times 10^{+01}$
362.97	301.26	320	168.69	2.84	$1.36 \times 10^{+01}$
362.68	301.31	320	168.10	2.81	$8.67 \times 10^{+00}$
362.35	301.37	320	167.57	2.78	$2.14 \times 10^{+00}$
362.36	301.36	320	167.14	2.79	$1.90 \times 10^{+00}$
362.61	301.47	320	167.53	2.80	$2.20 \times 10^{+00}$
		The second set of measurements			
T=290 K					
335.03	273.47	290	55.54	4.28	$1.22 \times 10^{+02}$
334.25	273.5	290	55.17	4.16	$5.38 \times 10^{+01}$
333.51	273.57	290	54.78	4.04	$2.72 \times 10^{+01}$
332.85	273.65	290	54.46	3.93	$1.65 \times 10^{+00}$
332.59	273.95	290	54.31	3.86	4.47×10^{-01}
333.28	273.69	290	54.60	3.99	$8.67 \times 10^{+00}$
T=300 K					
343.54	281.57	300	103.16	3.57	$1.91 \times 10^{+01}$
343.78	281.45	300	103.83	3.61	$2.32 \times 10^{+01}$
344.38	280.86	300	112.37	3.70	$6.51 \times 10^{+01}$
344.62	280.85	300	112.97	3.73	$8.35 \times 10^{+01}$
344.88	280.83	300	113.73	3.76	$9.62 \times 10^{+01}$
343.61	281.06	300	113.00	3.58	$1.63 \times 10^{+01}$
343.32	281.08	300	113.24	3.55	$1.55 \times 10^{+01}$
343.11	281.13	300	113.39	3.51	$7.74 \times 10^{+01}$
343.06	281.15	300	111.36	3.52	$2.70 \times 10^{+01}$
342.86	281.21	300	111.61	3.48	$8.15 \times 10^{+00}$
342.65	281.27	300	111.76	3.45	$5.85 \times 10^{+00}$
342.42	281.32	300	111.87	3.42	$2.56 \times 10^{+00}$
T=310 K					
353.73	290.66	310	140.12	3.24	$1.05 \times 10^{+02}$
352.91	290.69	310	139.68	3.16	$4.44 \times 10^{+01}$
351.19	391.12	310	138.27	2.97	5.14×10^{-01}
T=320 K					
364.60	299.18	320	202.19	3.04	$3.59 \times 10^{+02}$
364.16	299.21	320	202.19	3.00	$2.10 \times 10^{+02}$
363.73	299.29	320	202.19	2.96	$1.31 \times 10^{+02}$
363.30	299.40	320	201.71	2.92	$7.38 \times 10^{+01}$
362.86	299.48	320	201.00	2.88	$3.18 \times 10^{+01}$
362.41	299.58	320	200.29	2.84	$2.62 \times 10^{+01}$
361.91	299.65	320	199.69	2.79	$1.34 \times 10^{+01}$
361.46	299.76	320	199.19	2.75	$3.96 \times 10^{+00}$
360.98	299.83	320	198.45	2.71	6.68×10^{-01}

ation rates as a function of the saturation ratio are presented in Fig. 3. It can be seen that the experimental data are in qualitative agreement with the prediction of the classical theory of homogeneous nucleation (CNT).[30] However, the experimental points are about two orders in magnitude lower at 320 K and about three orders of magnitude lower at 290 K than the corresponding theoretical curves. In Fig. 3 we compare our experimental data also to the empirical nucleation rate function of Wölk *et al.*[31] Experimental data fit well at nucleation temperature of 320 K, but the deviation from the
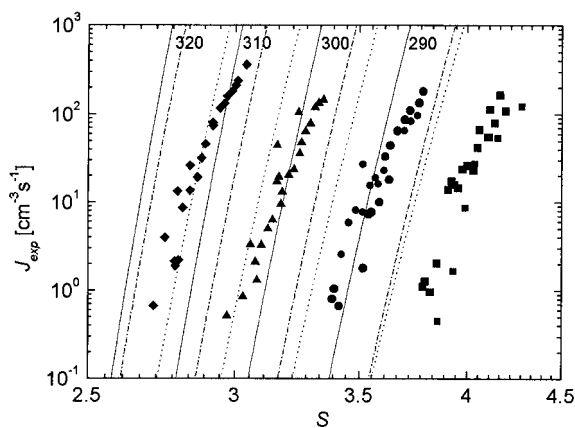
FIG. 3. The experimental nucleation rates J_{exp} as a function of saturation ratio S of water. Filled symbols (from left to right): diamonds—320 K, triangles—310 K, circles—300 K, and squares—290 K. Solid lines: CNT calculated for temperatures of 320, 310, 300, and 290 K. Dotted lines: Empirical nucleation rate function of Wölk et al. Dashed-dotted lines: Hale scaled theory with $\Omega = 1.47$.

empirical prediction increases toward the lower temperature isotherms and reaches about one order of magnitude at 290 K.

Comparison with the onset measurements

In Fig. 4 the data of this work are compared to the onset measurements of Wilson,[2] Volmer and Flood,[3] Heist and Reiss,[17] (separately for both carrier gases hydrogen and helium), Peters,[7] Mirabel and Katz,[18] and of Chukanov and Kuligin.[19] The ratio of the onset saturation ratio to the saturation ratio predicted by CNT theory is plotted as a function of the nucleation temperature. We have chosen the ratio S_{exp}/S_{CNT} on the vertical axis because Fig. 4 presents a combination of data obtained from both the expansion and the diffusion based devices, each of them using another value of the onset nucleation rate: e.g., Peters[7] takes 10^{11} cm^{-3} s^{-1} while this work uses only 2 cm^{-3} s^{-1} as the onset nucleation
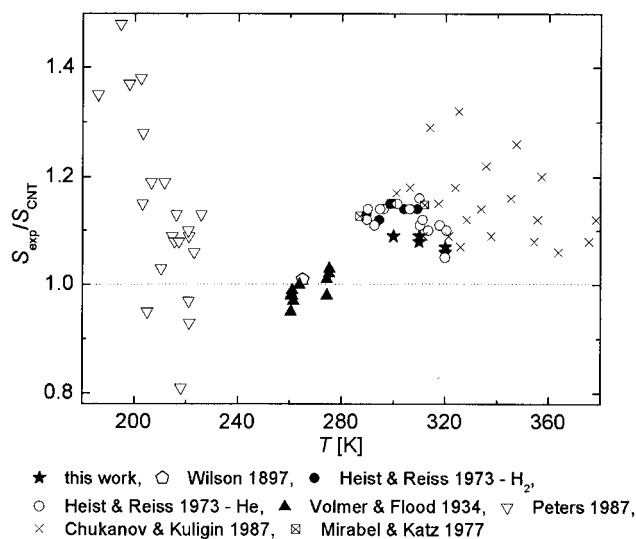
FIG. 4. Temperature dependence of the experimental saturation ratio to the critical saturation ratio calculated by the CNT.
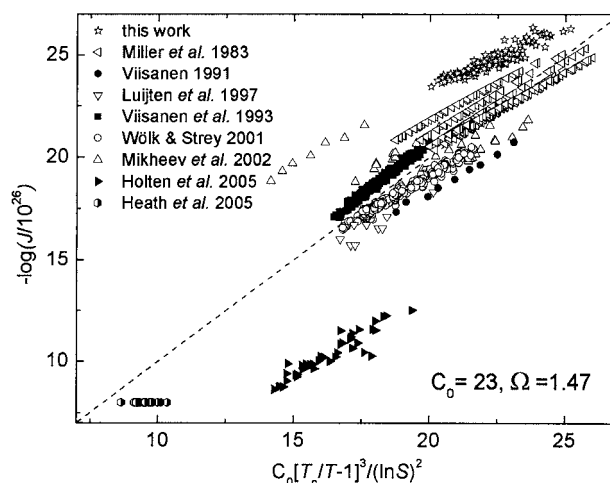
FIG. 5. A comparison of the scaled nucleation rates of water as a function of the scaled saturation ratio in the so-called Hale plot.

rates. The data presented here agree well with the data of Heist and Reiss,[17] Mirabel and Katz,[18] and of Chukanov and Kuligin;[19] all of these were obtained using diffusion chambers and over similar temperature ranges. All data from diffusion chambers fall just above the prediction of the CNT.[30] Experimental data of Wilson[2] and Volmer and Flood[3] sit on the dotted line symbolizing a perfect agreement with the CNT, while the data of Peters[7] lies on the dotted line only at higher nucleation temperatures but deviates from it toward lower temperatures.

Comparison with the nucleation rate measurements

In order to compare the experimental data from all available techniques in a consistent manner and keep the picture as clear as possible we have chosen a scaled model of nucleation suggested by Hale.[32–34]

The so-called Hale plot, see Fig. 5, produces two parameters $C_0[(T_c/T) - 1]^3/(\ln S)^2$ and Ω. The first parameter accounts simultaneously for the temperature and supersaturation dependencies in the exponent of the nucleation rate
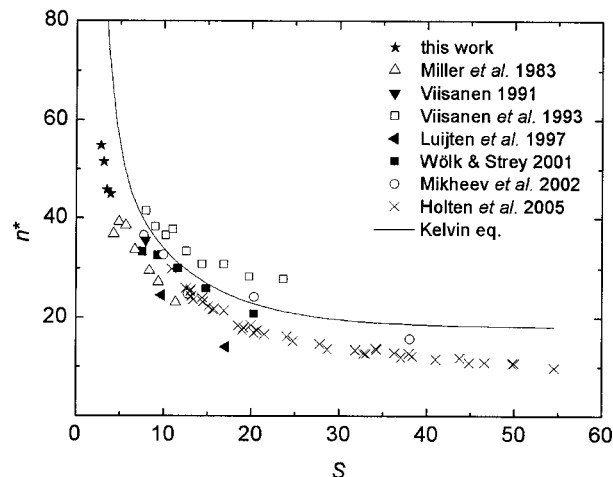
FIG. 6. Critical cluster sizes as a function of saturation ratio, the solid curve is a prediction of the critical cluster size calculated using the Kelvin equation.

expression. The parameter Ω is the excess surface entropy per molecule (divided by k) and is estimated from the experimental values of the surface tension. The effective value of Ω can be derived from C_0 by

$$\Omega = \left(\frac{3C_0}{16\pi} \times \ln 10 \right)^{1/3}. \tag{1}$$

This method offers a way to check the experimental data for consistency and also provides a basis to compare the experimental nucleation rates of any magnitude measured at arbitrary temperatures and supersaturations.

The "Hale plot" given on Fig. 5 uses only the nucleation rate data, the onset data are excluded. The compared rates scale well over a wide range of temperatures and supersaturations and the experimental data from this work seems to be consistent with the data of others. The resulting value of the parameter C_0 is 23 and the effective value of Ω is 1.47.

Critical cluster sizes

The critical cluster sizes can be calculated from the slopes of the nucleation rate isotherms according to the nucleation theorem,[35]

$$\left(\frac{\partial \ln J}{\partial \ln S} \right)_r \approx n^*. \tag{2}$$

In Eq. (2) n^* is the number of molecules in the critical cluster. One can also use the Kelvin equation to obtain the critical cluster radius r^*,

$$r^* = \frac{2\sigma v_{\text{liq}}}{kT \ln S}, \tag{3}$$

where v_{liq} is the volume of a liquid molecule and S is the experimental critical saturation ratio. Looking at the Kelvin equation, one sees that the critical cluster size depends both on the temperature and the saturation ratio. The number of molecules in the critical clusters is presented as a function of critical saturation ratio in Fig. 6. Our critical cluster sizes are lower than those predicted by the Kelvin equation. This is not unusual in TDCC measurements, e.g., of 1-butanol or 1-propanol[24,36] and is the case here for almost all data. Figure 7, the number of molecules in the critical cluster determined from our experiments as a function of the number of molecules in the critical cluster predicted by Kelvin equation, might be accessed via supplementary materials.[27] Again our measurements suggest a lower content of molecules in the critical cluster, see Fig. 7.

CONCLUSIONS

In this study two sets of nucleation rate isotherms (290, 300, 310, and 320 K) of water in helium were measured in a TDCC; the rates ranged from 3×10^{-1} to 3×10^2 cm^{-3} s^{-1}.

The obtained experimental results are in a reasonably good agreement with the prediction of the CNT. The experimental points are two and three orders of magnitude lower than the theoretical curves corresponding to the isotherms at 320 and 290 K, respectively. Our data compared to the em-

pirical nucleation rate function of Wölk et al.[31] fit well at the isotherm at 320 K, but at 290 K they are about one order of magnitude lower.

We compared our data to the measurements of others, both to the onset data and to the nucleation rate measurements. Data of this work agree well with the onset data obtained from diffusion chambers in a similar temperature range and are just slightly above the prediction of the CNT. All available experimental nucleation rate data are compared in the so-called Hale plot. The experimental data from this work seem to be consistent with the data of others and the whole dataset scales well over a wide range of temperatures and supersaturations.

Critical cluster sizes were estimated from the slopes of measured isotherms and compared to the prediction of Kelvin equation. Our measurements suggest somewhat lower content of molecules in the critical cluster than the theoretical prediction.

A short overview to the key physicochemical properties of water and possible sources of error are provided via supplementary materials online.[27] There was demonstrated that the application of any equation of liquid density, surface tension, and equilibrium vapor pressure used in the homogeneous nucleation studies until the present time will have an impact neither on the calculated profiles inside the TDCC nor on the obtained experimental results.

[1] A. Laaksonen, *Proceedings of the 15th International Conference on Nucleation and Atmospheric Aerosols*, edited by B. Hale and M. Kulmala (American Institute of Physics, Melville, NY, 2000), Vol. 7, p. 711.
[2] C. T. R. Wilson, Philos. Trans. R. Soc. London, Ser. A **189**, 265 (1897).
[3] M. Volmer and H. Flood, Z. Phys. Chem. Abt. A **170**, 273 (1934).
[4] L. B. Allen and J. L. Kassner, J. Colloid Interface Sci. **30**, 81 (1969).
[5] P. E. Wagner, and R. Strey, J. Phys. Chem. **85**, 2694 (1981).
[6] R. C. Miller, R. J. Anderson, J. L. Kassner, and D. E. Hagen, J. Chem. Phys. **78**, 3204 (1983).
[7] F. Peters, J. Phys. Chem. **91**, 2487 (1987).
[8] Y. Viisanen, "Experimental study of binary nucleation in the water n-propanol vapor mixture," Ph.D. thesis, Commentationes Physico-Mathematicae et Chemico-Medicae 133 (1991).
[9] Y. Viisanen, R. Strey, and H. Reiss, J. Chem. Phys. **99**, 4680 (1993).
[10] C. C. M. Luijten, K. J. Bosschaart, and M. E. H. van Dongen, J. Chem. Phys. **106**, 8116 (1997).
[11] J. L. Schmitt, K. V. Brunt, and G. J. Doster, *Proceedings of the 15th International Conference on Nucleation and Atmospheric Aerosols*, edited by B. Hale and M. Kulmala (American Institute of Physics, Melville, NY, 2000), Vol. 7, p. 51.
[12] Y. Viisanen, R. Strey, and H. Reiss, J. Chem. Phys. **112**, 8205 (2000).
[13] J. Wölk, Y. Viisanen, and R. Strey, *Proceedings of the 15th International Conference on Nucleation and Atmospheric Aerosols*, edited by B. Hale and M. Kulmala (American Institute of Physics, Melville, NY, 2000), Vol. 7, p. 7.
[14] J. Wölk and R. Strey, J. Phys. Chem. B **105**, 11683 (2001).
[15] C. H. Heath, K. Streletzky, B. E. Wyslouzil, J. Wölk, and R. Strey, J. Chem. Phys. **117**, 13 (2002).
[16] V. Holten, D. G. Labetski, and M. E. H. van Dongen, J. Chem. Phys. **123**, 104505 (2005).

[17] R. H. Heist and H. Reiss, J. Chem. Phys. **59**, 665 (1973).

[18] P. Mirabel and J. L. Katz, J. Chem. Phys. **67**, 1697 (1977).

[19] V. N. Chukanov and A. P. Kuligin, Teplofiz. Vys. Temp. **25**, 70 (1987).

[20] V. V. Beloded, G. A. Kirichewskij, and V. M. Nuzhnyi, J. Aerosol Sci. **20**, 1043 (1989).

[21] V. B. Mikheev, P. M. Irving, N. S. Laulainen, S. E. Barlow, and V. V. Pervukhin, J. Chem. Phys. **116**, 10772 (2002).

[22] J. Smolík and V. Ždímal, Aerosol Sci. Technol. **20**, 127 (1994).

[23] V. Ždímal and J. Smolík, Atmos. Res. **46**, 391 (1998).

[24] D. Brus, A.-P. Hyvärinen, V. Ždímal, and H. Lihavainen, J. Chem. Phys. **122**, 214506 (2005).

[25] J. L. Katz and B. J. Ostermier, J. Chem. Phys. **47**, 478 (1967).

[26] J. Smolík and J. Vašáková, Aerosol Sci. Technol. **14**, 406 (1991).

[27] See EPAPS Document No. E-JCPSA6-129-614841 for the error analysis, short overview, and comments to the key water physicochemical properties and Fig. 7. For more information on EPAPS, see http://www.aip.org/pubservs/epaps.html.

[28] A. Bertelsmann and R. H. Heist, J. Chem. Phys. **106**, 610 (1997).

[29] A. Bertelsmann and R. H. Heist, J. Chem. Phys. **106**, 624 (1997).

[30] R. Becker and W. Döring, Ann. Phys. **24**, 719 (1935).

[31] J. Wölk, R. Strey, C. H. Heath, and B. E. Wyslouzil, J. Chem. Phys. **117**, 4954 (2002).

[32] B. N. Hale, Phys. Rev. A **33**, 4156 (1986).

[33] B. N. Hale, Metall. Trans. A **23**, 1863 (1992).

[34] B. N. Hale, J. Chem. Phys. **122**, 204509 (2005).

[35] D. Kashchiev, J. Chem. Phys. **76**, 5098 (1982).

[36] D. Brus, V. Ždímal, and F. Stratmann, J. Chem. Phys. **124**, 164306 (2006).

[37] R. C. Reid, J. M. Prausnitz, and B. E. Poling, *The Properties of Gases and Liquids*, 4th edition (McGraw-Hill, New York, 1987).

[38] J. L. Katz, C. J. Scoppa II, N. G. Kumar, and P. Mirabel, J. Chem. Phys. **62**, 448 (1975).

[39] J. Vašáková and J. Smolík, Rep. Ser. Aerosol Sci. **25**, 1 (1994).

[40] L. Yaws, Chem. Eng. (Rugby, U.K.) **22**, 153 (1976).

[41] J. O. Hirschfelder, C. F. Curtiss, and R. B. Bird, *Molecular Theory of Gases and Liquids* (Wiley, New York, 1954), p. 539.

[42] J. d'Ans, A. Eucken, G. Joos, W. A. Roth, J. Bartels, P. Ten Bruggencate, H. Hausen, K. H. Hellwege, Kl. Schaefer, and E. Schmidt, *Landolt-Börnstein Zahlenwerte und Funktionen aus Physik-Chemie-Astronomie-Geophysik-Technik* (Springer-Verlag, Berlin, 1960), 6th Ed., Vol. 2, Pt. 2a, p. 32; Pt. 3, p. 421.

[43] L. W. Tilton and J. K. Taylor, J. Res. Natl. Bur. Stand. **18**, 205 (1937).

[44] Thermophysical Properties Research Center, *Data Book* (Purdue University, Lafayette, Ind., 1970), Vols. 2 and 3.